JCTC Journal of Chemical Theory and Computation

Article

pubs.acs.org/JCTC

Adaptive Resolution Simulation of MARTINI Solvents

Julija Zavadlav,[†] Manuel N. Melo,[‡] Ana V. Cunha,[‡] Alex H. de Vries,[‡] Siewert J. Marrink,*[,‡] and Matej Praprotnik*[,†]

[†]Laboratory for Molecular Modeling, National Institute of Chemistry, Hajdrihova 19, SI-1001 Ljubljana, Slovenia

[‡]Groningen Biomolecular Sciences and Biotechnology Institute and Zernike Institute for Advanced Materials, University of Groningen, Nijenborgh 7, 9747 AG Groningen, Netherlands

Supporting Information

ABSTRACT: We present adaptive resolution molecular dynamics simulations of aqueous and apolar solvents using coarse-grained molecular models that are compatible with the MARTINI force field. As representatives of both classes of solvents we have chosen liquid water and butane, respectively, at ambient temperature. The solvent molecules change their resolution back and forth between the atomistic and coarse-grained representations according to their positions in the system. The difficulties that arise from coupling to a coarse-grained model with a multimolecule mapping, for example, 4-to-1 mapping in the case of the Simple Point Charge (SPC) and MARTINI water models, could be successfully circumvented by using bundled water models. We demonstrate that the presented multiscale approach faithfully reproduces the structural and dynamical properties computed by reference fully atomistic molecular dynamics simulations. Our approach is general and can be used with any atomistic force field to be linked with the MARTINI force field.

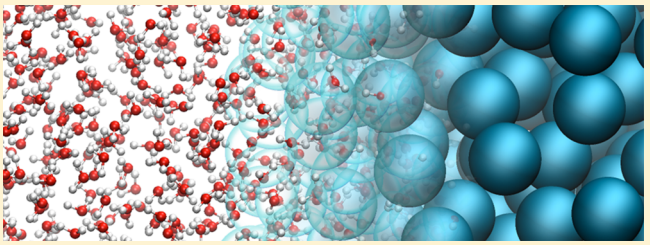

1. INTRODUCTION

Biomolecular systems are very challenging systems for computer simulation due to their complexity and related number of degrees of freedom. Despite the increasing computer power there are still many problems that are beyond the capabilities of current and near future computers. Coarse-graining techniques, where one reduces the number of degrees of freedom and retains only the relevant ones for the problem considered, have become increasingly important to bridge the vast span of spatial and temporal scales in these systems.[1−3] A popular biomolecular coarse-grained (CG) force field is MARTINI,[4,5] which has been parametrized in a systematic way, based on the reproduction of partitioning free energies between polar and apolar phases of a large number of chemical compounds. The MARTINI force field uses a 4-to-1 mapping, that is, on average four heavy atoms are represented by a single interaction center. In this way, the number of particles and corresponding degrees of freedom is considerably reduced, while still retaining chemical specificity. This approach allows for a wide range of applications, for example, lipid self-assembly, peptide membrane binding, protein−protein recognition, etc.[6]

However, often we need a high resolution in a certain subdomain of the total system and multiscale modeling approaches are the most efficient way to tackle these situations.[7−11] In multiscale methods different domains of the systems are modeled using different levels of detail where molecules can either stay fixed in separate resolution domains[12−20] or freely move between them.[8,21−25] One of the most advanced methods from the latter class of approaches is the Adaptive Resolution Scheme (AdResS),[8,26−31] which allows for concurrent coupling from quantum all the way to continuum length scales of soft matter systems. Thus far, one of the limitations of this multiscale scheme has been that it could only be applied using 1-to-1 molecular CG mapping schemes; that is, one fine-grained molecule is mapped to one CG molecule.[8] When several small molecules, such as water molecules, are mapped to one and the same CG bead problems arise because the correspondence of the coordinates between fine- and coarse-grained representations becomes meaningless when the fine-grained molecules diffuse too far from each other. For example, in the case of water this happens on a picosecond time scale. In order to be able to perform adaptive resolution simulations using multiscale schemes such as AdResS, bundled water models[32,33] have been recently introduced where the relative movement of water molecules that are mapped to the same CG bead was restricted using harmonic springs.

Here, we report the details of adaptive resolution simulations of aqueous and apolar solvents using the atomistic (AT) GROMOS[34] and CG MARTINI force fields. We simulate liquid water and butane at ambient conditions, allowing the solvent molecules to adaptively change their level of resolution from AT to CG and vice versa. We observe within our error bars no differences between the structural and dynamical properties of our solvents in the adaptive resolution approach compared to reference full-blown molecular dynamics simu-

Received: February 20, 2014
Published: April 23, 2014

   dx.doi.org/10.1021/ct5001523 | J. Chem. Theory Comput. 2014, 10, 2591−2598

lations. Given that MARTINI force field parameters are available for many solvents, the ability to interface with the AdResS approach opens up a wide range of potential multiscale applications.

2. METHODS

2.1. AdResS. To link AT and CG models we apply the Adaptive Resolution Scheme (AdResS).[8,26] In this scheme, molecules can freely exchange resolution through a transition regime containing hybrid molecules (see Figure 1). The total

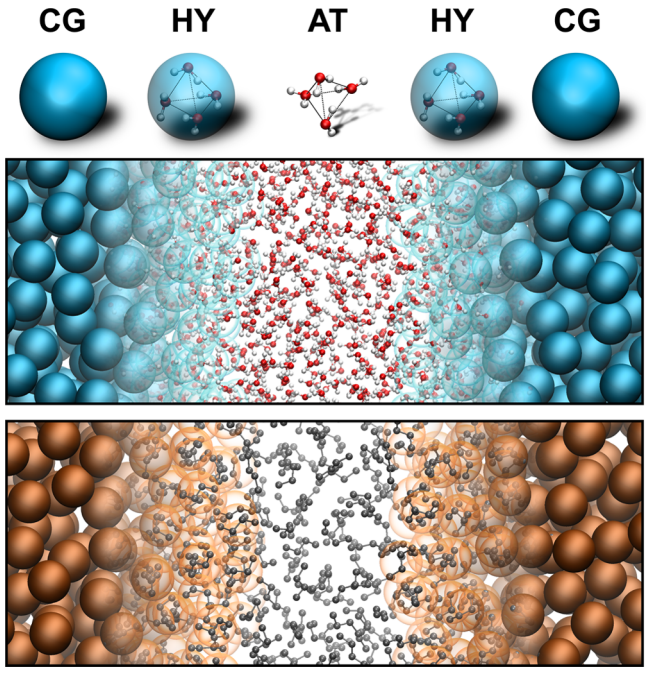

Figure 1. Multiscale representation of water and butane systems, with resolution changing from atomistic (AT, center) to coarse-grained (CG, edges); the molecules change their representation on-the-fly as they diffuse through the transition hybrid (HY) regions. Top: illustration of different resolutions for an individual water cluster; in the AT region the bundled water model[32] is used, where four SPC water oxygens are connected by semiharmonic springs; in the CG region the four water molecules are grouped into a single particle with MARTINI[4] water model parameters. Middle: Depiction of a bundled water AdResS system. Bottom: depiction of a butane AdResS system, coupling a united-atom representation to a MARTINI one.

force acting on a bundle—or molecule, in the case of butane where a 1-to-1 molecule CG mapping is used—α is

$$\mathbf{F}_\alpha = \sum_{\beta\neq\alpha} w(X_\alpha)w(X_\beta)\mathbf{F}^{\mathrm{at}}_{\alpha\beta} + \sum_{\beta\neq\alpha} [1 - w(X_\alpha)w(X_\beta)]\mathbf{F}^{\mathrm{cg}}_{\alpha\beta} - \mathbf{F}^{\mathrm{TD}}(X_\alpha) \quad (1)$$

where $\mathbf{F}^{\mathrm{at}}_{\alpha\beta}$ and $\mathbf{F}^{\mathrm{cg}}_{\alpha\beta}$ are the forces between bundles α and β, obtained from the explicit AT and CG potentials, respectively. The smooth transition between different resolution regions is ensured by a weighting function w that depends on the X position of the bundle's center of mass (COM). This function is defined in such a way that $w = 1$ corresponds to the AT region and $w = 0$ to the CG region, whereas the values $0 < w < 1$ correspond to a hybrid (HY) region. An additional thermodynamic (TD) force $\mathbf{F}^{\mathrm{TD}}$ is used to compensate for the difference in the chemical potential at different levels of resolution and to achieve a uniform density profile throughout the simulation box.[35,36]

The AdResS method requires a thermostat that will couple locally to the particle motion and supply or remove the latent heat caused by the switch of resolution.[8] In this study, we used two local thermostats, that is, the Langevin and linear momentum preserving dissipative particle dynamics (DPD)[37,38] thermostats.

2.2. Hybrid Bundled-SPC/MARTINI Water. We have developed a multiscale water model with a 4-to-1 mapping, where atomistic water, composed of a bundle of four SPC water molecules,[32] is coupled to the MARTINI CG water,[4] as illustrated in Figure 1. It is known that the lifetime of tetrahedral clusters in water is well below 1 ps.[8] Hence, water molecules initially in a tetrahedral cluster will over time diffuse away from one another. Consequently, multiple water molecules can not be easily coupled to a single CG particle as such coupling would require water molecules to be redistributed into CG beads on the fly. Coupling can be simplified with a constant mapping; that is, CG particles are mapped to the same four water molecules during the total simulation run. In this case, one has to keep the water molecules within one CG particle from drifting apart. To this end, springs are added between all oxygen atoms within a bundle and modeled with an attractive semiharmonic potential

$$V_{\mathrm{spring}} = \begin{cases} \frac{1}{2}k_s(r_{ij} - r_0)^2, & r_{ij} > r_0 \\ 0, & r_{ij} < r_0 \end{cases} \quad (2)$$

where k_s represents the force-constant, r_{ij} the distance between oxygen atoms, and r_0 the equilibrium distance between oxygen atoms, which is set to 0.3 nm. We consider two different force-constants which represent two different bundling models:[32] model 1 with k_{s1} = 1000 kJ/(mol nm^2) and model 2 with k_{s2} = 4000 kJ/(mol nm^2). Because the springs between oxygen atoms will to some extent change the properties of the system, we use modified oxygen−oxygen Lennard-Jones (LJ) parameters that have been developed[32] to have the bundled models reproduce the properties of SPC water. For the solvent in the low resolution regime we employ the standard MARTINI water model.[4]

Hybrid bundled-SPC/MARTINI water simulations were performed using the ESPResSo++ software package.[39] We used the standard Velocity-Verlet integrator with a time step of 1 fs, dictated by the high frequencies of the AT interaction potentials; as remarked elsewhere,[40] performance can be improved by simulating the CG region at larger timesteps without loss of stability, given the softer nature of the CG potentials. Water geometry was constrained with the SETTLE[41] algorithm. The nonbonded interactions were calculated with LJ and Coulomb interactions within a cutoff distance r_c = 1.4 nm. For the electrostatic interactions beyond the cutoff we used a reaction-field correction,[42,43] with a dielectric constant of 54.[32] Atomistic LJ interactions were capped for distances smaller than 0.2 nm. All simulations were performed under NVT conditions in an orthorhombic simulation box with periodic boundary conditions and minimum image convention. We employed the Langevin thermostat with a coupling constant of 1.0/ps and the DPD thermostat with a coupling constant of 0.025 au/ps and a cutoff radius equal to the cutoff radius of nonbonded interactions. Temperature was coupled to either 300 or 323 K. The TD

dx.doi.org/10.1021/ct5001523 | J. Chem. Theory Comput. 2014, 10, 2591−2598

force that acts on the COM of bundles in the HY region is calculated in an iterative procedure in an inversely proportional fashion to the density gradient along the direction of resolution change as described in the literature.[35,36] On average, 15 iterative steps were used for each TD force convergence. To speed up the iteration procedure we ran simultaneously at each step several simulations with different proportionality factors and chose the best one for the next iteration.

The adaptive resolution simulation box (11.2 × 2.8 × 2.8 nm^3) was set up as depicted in Figure 1. The AdResS method allows the use of different geometric boundaries between resolution regions. Here, we split the system along the *x*-axis, so that a 4.2 nm-wide AT region is at the center of the simulation box. Two HY regions, of a width of 1.4 nm each, flank the AT region.

The initial system of bundled water molecules was prepared by first equilibrating a system of 2796 SPC water molecules. A series of short atomistic simulations was then run. At each step, the distances between oxygen atoms were measured, and if they were small enough—and the oxygen atoms were connected to less than three other oxygen atoms—semiharmonic springs were added between them (see eq 2). This process was repeated until all the four-water bundles were formed. After equilibration, trajectories of 10 ns were computed. Three different sets of simulations were performed: fully atomistic, fully coarse-grained, and AdResS multiscale simulations.

To illustrate the compatibility of the AdResS scheme with different MD implementations, the same system was also simulated using the GROMACS 4.6.4 software package (modified for SPC stability; see the Supporting Information), for which an implementation of the AdResS scheme is available.[44] In this case; only the second bundling model was simulated, using a leapfrog integration scheme and temperature-coupling to 323 K using a Langevin thermostat. Coupling, time step, and force calculation parameters were as described for the ESPResSo++ implementation above.

2.3. Hybrid Liquid Butane. We also performed AdResS simulations of butane, under conditions where it is liquid, coupling between the GROMOS 53a6 united-atom representation[34] and the MARTINI CG one. This system is simpler than that of hybrid water both because only LJ nonbonded interactions are present and because there is a one-to-one mapping of butane molecules to CG beads. These simulations are relevant to demonstrate the ability of the AdResS scheme to also couple hydrophobic solvents and, in this particular case, to couple two subsystems at very different pressures.

Butane simulations were performed solely using the GROMACS 4.6.3 software package. A leapfrog integrator with Langevin friction and noise was used, with a time step of 3 fs and a coupling constant of 0.1/ps to a temperature of 323 K. The GROMOS 53a6 united-atom model was used for the atomistic representation of the molecules, and the MARTINI model for their CG counterparts. Atomistic bonds were left unconstrained. No charges were present in the system. LJ interactions were evaluated in a twin-range scheme, with forces between particles up to 0.8 nm apart being calculated every step, and those between particles 0.8 to 1.4 nm apart being calculated every 10 steps. The atomistic LJ potential is cutoff at 1.4 nm[34] whereas the CG one is modified so that forces are shifted to zero between 0.9 and 1.2 nm.[4] This setup reproduces the settings used for parametrization of the GROMOS 53a6 force field, but due to implementation limitations that do not allow multiple neighbor-searching schemes, it differs slightly from the parametrization settings for the MARTINI force field (in which case, instead of a twin-range approach, forces up to 1.2 nm were calculated every step). Because, however, the MARTINI parametrization time step is of at least 20 fs, the use of a twin-range scheme with a time step of 3 fs should have minimal impact on results. The TD force converged after 71 iterative steps of 3 ns each. The VOTCA software package,[45] version 1.3, was used for automation of the process, but the proportionality factor between the density gradient and the applied force at each iteration was reduced manually along the process so as to prevent overcorrection.

A cubic system of 10.0 × 10.0 × 10.0 nm^3 was used, with AdResS regions split along the *x*-axis. A 3 nm-wide AT region is at the center of the box, flanked by two 1.5 nm-wide HY regions. The remaining 4 nm correspond to a single contiguous (due to periodicity) CG region. The starting conformation for the AdResS simulations was obtained from a system with the same volume and with 7396 atomistic butane molecules, preequilibrated for 3.5 ns, at 323 K.

Fully AT and CG systems, with the same volume and number of butane molecules were also simulated. Atomistic time step and force-calculation parameters were as described for the AdResS system whereas the CG system was simulated with a 30 fs time step and a 1.2 nm single-range neighbor searching scheme updated every 10 steps.

3. RESULTS AND DISCUSSION

3.1. Hybrid Bundled-SPC/MARTINI Water. To validate the correct coupling of hybrid bundled-SPC/MARTINI water model the structural and dynamic properties of the system were assessed at two temperatures, T = 300 K and T = 323 K, and using the Langevin and DPD thermostats (the results for the DPD thermostat are included in the Supporting Information). In Figure 2, we show the radial distribution function (RDF) of oxygen atoms and COM of bundles for both bundling models at T = 300 K. RDFs from atomistic simulations were compared to those of the AdResS simulation, only taking into account bundles within the AT region. Likewise, the RDF of water beads, obtained from a coarse-grained simulation, was compared to that of the bundle COMs in the CG region of the AdResS simulation (Figure 2). The local structure in the AT and CG AdResS domains is the same as in the respective reference atomistic/coarse-grained simulations and is in agreement with those reported in the literature.[32] Simulations at T = 323 K give identical results. The discrepancy between the RDF peak widths of bundle COMs and CG beads (Figure 2B and 2C) reflects the known overstructured nature of MARTINI water.[32] This shows that the AT and CG models need not have matching properties for a successful coupling with AdResS.

The applied TD forces are shown in Figure 3 for both models and temperatures. While the two models require TD forces of different magnitude, the force profile shapes are similar. See the Supporting Information for TD forces with the DPD thermostat. The resulting homogeneous density across different resolution regions is evident from the normalized density profile (NDP) of bundle COMs along the *x*-axis (the direction of resolution change). For both models and temperatures the NDPs are shown in Figure 3. As a reference, we also show the NDPs for the case where the thermodynamic force is omitted from the AdResS force scheme. It can be seen that the computed TD force correctly compensates for the large

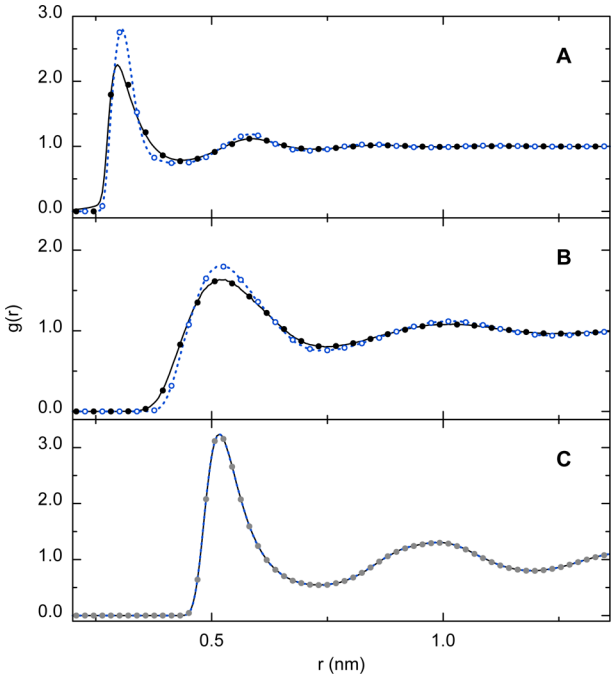

Figure 2. RDF of oxygen atoms (A), bundle COMs (B), and CG beads (C) for bundled water models 1 and 2 (in black and dotted blue, respectively) at 300 K. RDFs were obtained from the AT region for the oxygen and bundle COMs (A and B), or from the CG region for the CG beads (C). The RDFs from the reference AT and CG simulations are overlaid as circles in the relevant plots (A and B, and C, respectively), with very good agreement.

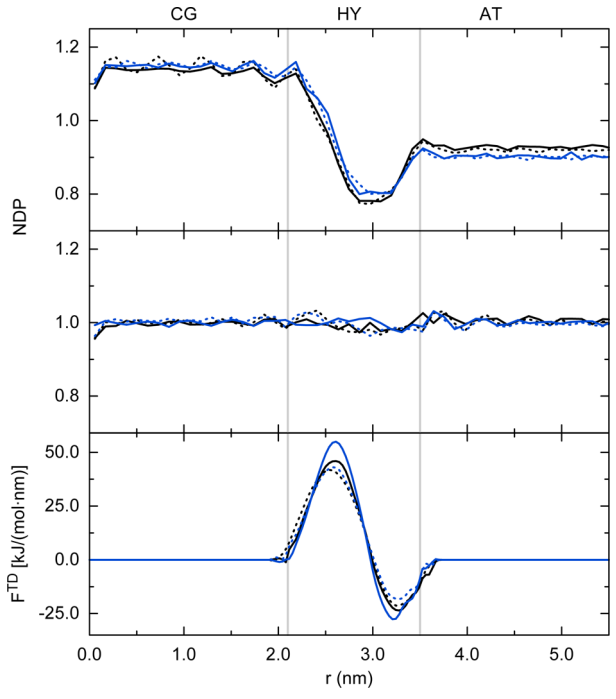

Figure 3. Normalized density profile of bundled water models 1 and 2 at T = 300 K and T = 323 K (black and blue lines indicate models 1 and 2, respectively; full and dotted lines indicate T = 300 K and T = 323 K, respectively). The top plot shows the case without TD force, while the middle plot shows the case with TD force. Error bars are approximately 1%. The bottom plot shows the applied TD force for each model and temperature. Vertical lines show the boundaries of the AT, HY, and CG regions.

density fluctuations that occur when the TD force is not included in the scheme.

Note that if the TD force is not computed accurately enough density oscillations appear in the HY region. These oscillations reflect the grain size of the MARTINI model as well as that of the bundled water model itself (the period is almost 0.5 nm for both systems corresponding to the period of the oscillations we observed in the HY region — data not shown). Normally, these oscillations do not occur if one plots density distributions along a particular axis in one's system, unless the system is somehow confined. Adjacent to a hard wall, for instance, very pronounced density oscillations would show up that slowly decay away from the interface. In our case, we have two interfaces, the AT/HY interface and the HY/CG interface. Both of these interfaces induce order (although not as much as a hard wall would, of course). In the simulations presented here, we have used a HY region of 1.4 nm width, which approximately fits three layers of bundled/MARTINI water and therefore reinforces the structuring effect. A HY region of a width that is not a multiple of the bundled/MARTINI water molecule size should weaken the structuring effect.[40] In any case, the application of an appropriate TD force, as our results demonstrate, can prevent any such water structuring.

Another potential problem due to artificial ordering is the freezing of water. MARTINI water is known to freeze between 280 and 300 K.[4] In particular, rapid freezing occurs when a nucleation site is already present; the surface of the hybrid region may act as one. In our simulations freezing never occurred, even upon large structuring due to insufficient TD correction. Freezing might also have been prevented by having a fixed system volume, which could hinder the phase transition. In any case, applications requiring lower temperatures could, at least in principle, face the possibility of the CG subsystem freezing. In these situations, and as proposed for the pure MARTINI case,[4] a small proportion of the water beads can be assigned a bigger CG representation. These particles break the lattice and lower the freezing temperature. Their inclusion in the AdResS treatment should be considered as the addition of a second solvent: independent TD forces must be obtained for the two different water particle types, as detailed elsewhere.[35]

When atomistic water molecules approach a neutral fluid surface (as happens upon entering the CG water region), the hydrogen bond network formed among the atomistic molecules can be strongly perturbed. As a result, the atomistic molecules near the resolution interface could orient and behave differently from the bulk. However, this spurious effect can be avoided by using an appropriate HY domain between the AT and CG domains. It has been shown that this perturbation extends around 1 nm into the atomistic water layer.[46,47] This distance is smaller than the width of our HY region. Results depicted in Figure 4 for both water models at 300 K show that indeed the presence of the HY regime removes any such orientational bias before the AT region is reached. The figure shows the average orientations of three vectors, namely the dipole moment of a water molecule, the vector perpendicular to the plane of the molecule and the vector joining the two hydrogen atoms of the molecule, as a function of the coordinate x spanning across the two resolutions in the simulation box. We denote the angles formed by these vectors and the normal vector pointing toward our coarse-grained water liquid as α, β, and γ, respectively.[47] The average orientations of the vectors are quantified by the average cosine values of these angles.

dx.doi.org/10.1021/ct5001523 | J. Chem. Theory Comput. 2014, 10, 2591−2598

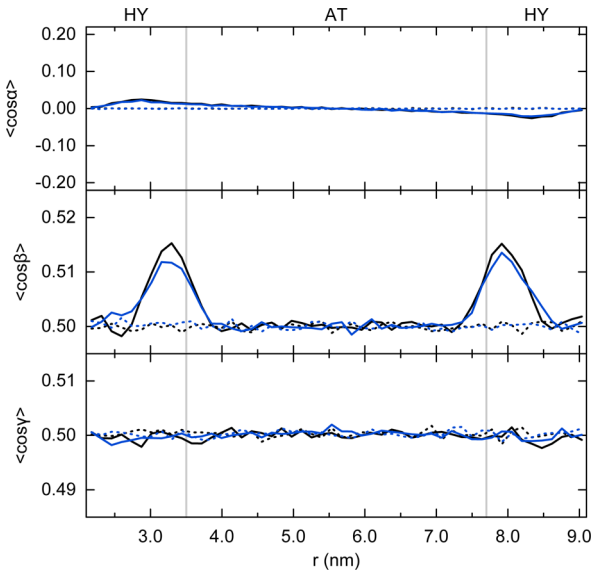

Figure 4. Average cosine value of the angle formed by the dipole vector (α, top panel), the vector joining the two hydrogen atoms of a molecule (β, middle panel) and the vector normal to the plane of a molecule (γ, bottom panel) with the interface normal vector pointing toward the CG region as a function of the x-coordinate in the simulation box.[47] Results for both water models simulated at 300 K compared to reference all-atom simulations of the same two models (model 1 in black and model 2 in blue; AdResS simulations as full lines and reference all-atom ones as dotted ones). The results demonstrate that after crossing the HY region the water molecules have a random orientation in the AT domain. The HY domain thus neutralizes the orientational effect of the CG domain so that the water in the AT region has the same structural properties as the all-atom bulk water.

As the bundles approach the CG domain from the AT side the electrostatic interactions are gradually turned off. This should have an effect on the bundle's dipole moment distribution in the HY region as indeed is evident from our results, displayed in Figure 5. The distribution is, as expected, shifted toward lower dipole moments compared to the distribution in the AT region.

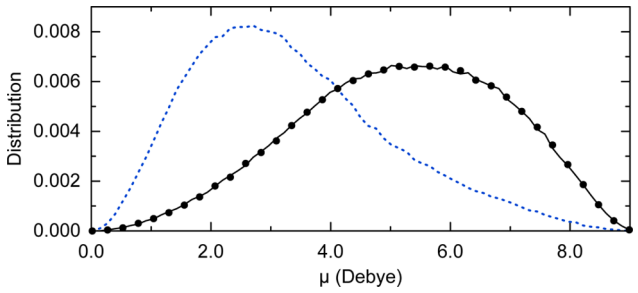

Figure 5. Distribution of bundle's dipole moment in the AT (black) and HY (dotted blue) regions for model 1 at T = 300 K. The distribution in the AT region closely matches the corresponding one from the reference all-atom simulation (black circles).

We have also computed the static dielectric constant ϵ from fluctuations of the total dipole moment as[48]

$$\epsilon = \frac{1 + [(<M^2> - <M>^2)/3\epsilon_0 V K_B T]\,[2\epsilon_{RF}/(2\epsilon_{RF}+1)]}{1 - [(<M^2> - <M>^2)/3\epsilon_0 V K_B T]\,[1/(2\epsilon_{RF}+1)]} \quad (3)$$

where M is the total dipole moment of the system, V is the total volume of the system, k_B is the Boltzmann constant, and T is the absolute temperature. The results are shown in Table 1. Note that the values for both bundled-SPC water models are in better agreement with the experimental ones than the original SPC water model, which gives under the same conditions at T = 300 K the dielectric constant of 40.2 ± 0.5.

Table 1. Diffusion Coefficients and Dielectric Constants for Models 1 and 2 at Temperatures T = 300 K and T = 323 K[a]

model	T [K]	D (AT) [10^{-9} m^2 s^{-1}]	D (CG) [10^{-9} m^2 s^{-1}]	ϵ (AT)
1	300	1.8	1.8	76.7
2	300	1.8	1.8	77.3
1	323	2.1	2.0	65.3
2	323	1.9	2.0	68.5

[a]Results include the finite-size correction:[49,50] 0.07 × 10^{-9} m^2 s^{-1} for model 1, and 0.06 × 10^{-9} m^2 s^{-1} for model 2; the viscosities used for the evaluation of finite size correction are from ref 32. Error bars are approximately 5% and 1% for diffusion coefficients and dielectric constants, respectively.

The diffusion coefficients D from the mean square displacement of bundle COMs were also computed from the AdResS simulation (Table 1). Both models give similar diffusion constants that are, as reported earlier,[32] lower than that of SPC water (4.5 × 10^{-9}m^2 s^{-1} at 301 K[51]). Diffusion is expected to be slower due to the larger hydrodynamic radius of the bundles versus single SPC molecules. A better comparison can be made with the COM of four independently diffusing SPC water molecules:[32] this corresponds to a bundling with zero bundling potential, which diffuses 4-fold slower than SPC[32]—much closer to the diffusion of the bundled models. In the bundled water systems the diffusion constants of the coarse-grained and all-atom subsystems were similar (Table 1). In other situations—see the case of butane below—diffusion may differ to some extent across subsystems. A position-dependent local thermostat can then be used to match the dynamics of both models.[8,52] If the thermostat coupling constants are small in comparison to intrinsic friction, as was the case for the bundled water AdResS simulations, diffusion will not be affected by application of the thermostat.

In Figure 6 we show the time evolution of a diffusion profile of bundled water COMs to demonstrate that the bundles can freely move across adaptive resolution regions. The bundles are initially in a slab within the AT, CG, or HY region but diffuse in time throughout the whole simulation box. Particles from the HY region spread out equally to the AT and CG region, which is in accordance with our previous finding of similar diffusion coefficients in both regions.

3.1.1. Simulations Using GROMACS. When using the GROMACS implementation,[44] simulations of hybrid water became unstable due to occasional atom overlaps. The cause of this behavior was traced to the implementation of an aspect of the AdResS scheme: forces felt in the HY region must be limited at low interparticle distances; this prevents singularities from occurring when atoms overlap as COMs diffuse from the CG to the HY region[26] (see the Supporting Information for further details). In GROMACS, this is implemented as a capping at a constant force value. However, in the particular case of SPC, this approach offsets the attractive/repulsive balance between water oxygens and hydrogens (note that SPC hydrogens lack a LJ repulsion term). This results in unphysical and unstable molecular overlaps. The problem was solved by replacing this capping scheme by a distance-based force

dx.doi.org/10.1021/ct5001523 | J. Chem. Theory Comput. 2014, 10, 2591−2598

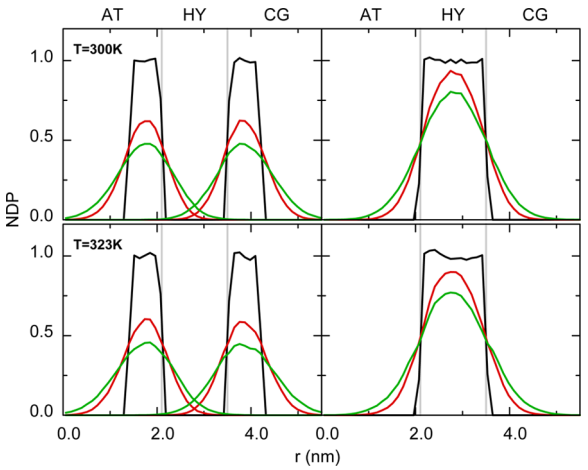

Figure 6. Diffusion of centers of mass of bundled waters for model 1 at 300 (top) and 323 K (bottom). Left: Normalized density distributions of particles at time t = 0 ps (black) in a slab with width 0.7 nm in the CG or AT region and at times t = 50 ps (red) and t = 100 ps (green). Right: The same time evolution for particles initially in the HY region.

truncation approach similar to the ESPResSo++ implementation. Since the results overlap with those of the ESPResSo++ package they are presented in the Supporting Information, together with a description in greater detail of the modified force capping scheme.

3.2. Hybrid Liquid Butane. The butane system was also successfully simulated with the AdResS multiscale coupling. As with the bundled water simulations, free AdResS simulations of the butane system resulted in a density imbalance along the x coordinate of the box. The same iterative procedure as described above was performed to arrive at a TD force that compensates for this effect, as seen in Figure 7. It should be noted that at this volume and temperature the pure AT and CG systems have very different pressures (2778.5 ± 0.5 and 200.79 ± 0.02 bar, respectively), which still could be balanced by the TD force approach. In addition, the structural properties of

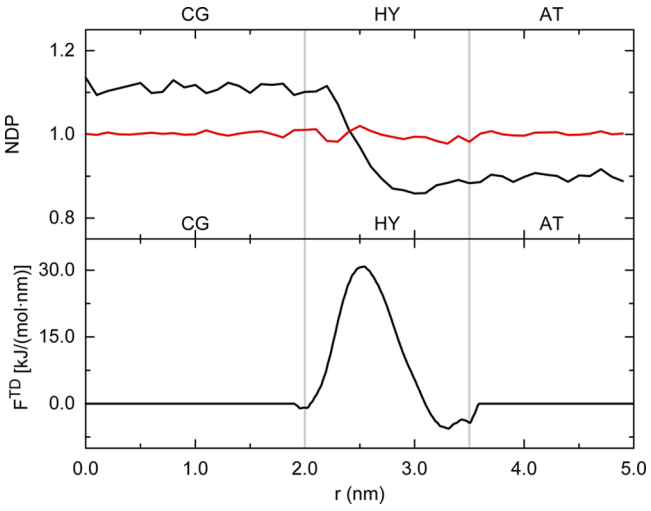

Figure 7. Top: normalized density profile of butane COMs in an AdResS simulation as a function of the x-distance to the center of the box. A density imbalance is visible in a free AdResS simulation (black), which is successfully compensated for when an appropriate TD force is used (red). Bottom: the used TD force. Vertical lines show the boundaries of each resolution region.

either the AT or the CG regions were very well preserved compared to reference atomistic and coarse-grained simulations (Figure 8). In contrast with water models, butane simulations

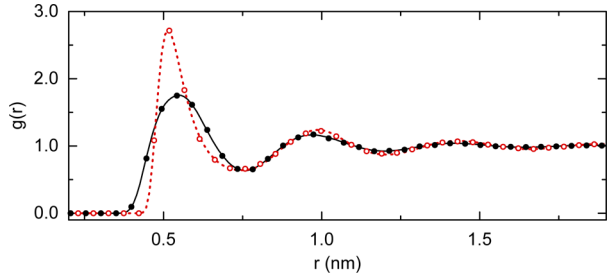

Figure 8. RDF of the COMs of the butane molecules in the AdResS system, from either the AT slab (black) or the CG one (dotted red). RDFs from reference AT and CG systems are overlaid in circles, with very good agreement.

could be performed with the unmodified force-capping method of GROMACS 4.6.4; no atom overlaps were observed in this case, due to repulsive LJ terms in all atomistic nonbonded interactions.

The use of the AdResS scheme did not present any diffusion barrier to the butane molecules. It can be seen in Figure 9 that

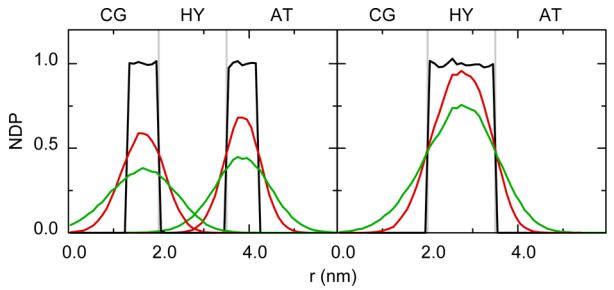

Figure 9. Diffusion of butane centers of mass in an AdResS simulation, starting from either 0.7 nm slabs next to the HY region (left) or in the entire HY region itself (right). Normalized density distributions at times 0, 30, and 90 ps are shown in black, red, and green, respectively. Vertical lines show the boundaries of each resolution region.

molecules diffuse freely from the HY region into either CG or AT region, albeit slightly faster to the former. This is one of the expected consequences of coupling an atomistic system to a coarse-grain one, where overall softer potentials lead to lower friction and increased diffusion speeds.

Finally, we looked at the influence of the coupling scheme on the isotropic orientation of the butane molecules and their internal structure, as reflected by their asphericity and radius of gyration, respectively. Asphericity (Δ) is defined as elsewhere:[53]

$$\Delta = \frac{3}{2}\frac{\left[\sum_{i=1}^{3}\left(\lambda_i - \frac{tr\mathbf{T}}{3}\right)^2\right]}{(tr\mathbf{T})^2} \quad (4)$$

where $\mathbf{T}$ is the inertia tensor of the collection of particles, and λ_i the eigenvalues of $\mathbf{T}$—or the squares of the three principal radii of gyration of the particle cloud. Equation 4 was applied simultaneously to the atoms of all the molecules whose COM fell within a 0.2 nm bin and after centering all the binned COMs (it is easy to see that an anisotropic orientation will produce, after centering, a spherical particle cloud).

dx.doi.org/10.1021/ct5001523 | J. Chem. Theory Comput. 2014, 10, 2591−2598

Both the asphericity and average radius of gyration show a very slight departure from isotropic behavior in the hybrid region (Figure 10). Similarly to what is observed with the

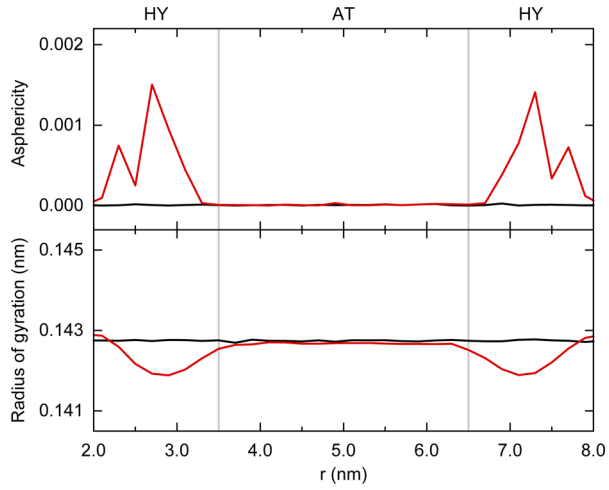

Figure 10. Dependence of orientational preference and intramolecular organization of butane along the *x* axis in an AdResS system (red) or a reference atomistic one (black). Top: asphericity (as per eq 4) of butane atoms in each *x* bin, after centering the molecules' COM. A departure from isotropic orientation results in asphericity values larger than 0. Bottom: molecular radius of gyration, averaged after binning in *x*. In both plots, a small deviation (<1%) from isotropic behavior can be observed when compared to the atomistic system. These imbalances become negligible within the AT region.

bundled water (Figure 4) these imbalances—which are smaller than 1% in magnitude—are resolved by the point the system reaches the atomistic region and will therefore not affect its dynamics.

4. CONCLUSIONS

In this work, we have applied the AdResS scheme to the multiscale coupling of both aqueous and apolar solvents. The difficulties that arise from coupling to a coarse-grain model with a multimolecule mapping—the case of the MARTINI water—could be successfully circumvented by using bundled water models. We have used different methods for thermostatizing the system preserving solvent structure and dynamic properties. Finally, consistent results were obtained across AdResS implementations in different molecular dynamics software packages, highlighting the broad applicability of this multiscaling approach. An example application of a successful adaptive resolution simulation of a solvated atomistic protein in MARTINI water has been recently published.[40]

■ ASSOCIATED CONTENT

Supporting Information

Results and details on the simulations of bundled-SPC/MARTINI water with the DPD thermostat and adaptive resolution simulations using GROMACS. This material is available free of charge via the Internet at http://pubs.acs.org/.

■ AUTHOR INFORMATION

Corresponding Authors

*Email: s.j.marrink@rug.nl.
*Email: praprot@cmm.ki.si.

Notes

The authors declare no competing financial interest.

■ ACKNOWLEDGMENTS

We thank M. Karttunen and K. Kremer for useful discussions. M.P. and S.J.M. acknowledge hospitality at KITP where this collaboration was initiated. This research was supported in part by the National Science Foundation under Grant No. NSF PHY11-25915. J.Z. and M.P. acknowledge financial support through the grants J1-4134 and P1-0002 from the Slovenian Research Agency. Support from The Netherlands Organization for Scientific Research (NWO) is thankfully acknowledged (Veni grant 722.013.010 to M.N.M).

■ REFERENCES

(1) Noid, W. G. *J. Chem. Phys.* **2013**, *139*, 090901.
(2) Ingólfsson, H. I.; Lopez, C. A.; Uusitalo, J. J.; de Jong, D. H.; Gopal, S.; Periole, X.; Marrink, S. J. *WIREs Comput. Mol. Sci.* **2014**, *4*, 225−248.
(3) Baaden, M.; Marrink, S. J. *Curr. Opin. Struct. Biol.* **2013**, *23*, 878−886.
(4) Marrink, S. J.; Risselada, H. J.; Yefimov, S.; Tieleman, D. P.; de Vries, A. H. *J. Phys. Chem. B* **2007**, *111*, 7812−7824.
(5) Monticelli, L.; Kandasamy, S. K.; Periole, X.; Larson, R. G.; Tieleman, D. P.; Marrink, S. J. *J. Chem. Theory Comput.* **2008**, *4*, 819−834.
(6) Marrink, S. J.; Tieleman, D. P. *Chem. Soc. Rev.* **2013**, *42*, 6801−6822.
(7) Kamerlin, S. C. L.; Vicatos, S.; Dryga, A.; Warshel, A. *Annu. Rev. Phys. Chem.* **2011**, *62*, 41−64.
(8) Praprotnik, M.; Delle Site, L.; Kremer, K. *Annu. Rev. Phys. Chem.* **2008**, *59*, 545−571.
(9) Murtola, T.; Bunker, A.; Vattulainen, I.; Deserno, M.; Karttunen, M. *Phys. Chem. Chem. Phys.* **2009**, *11*, 1869−1892.
(10) Peter, C.; Kremer, K. *Soft Matter* **2009**, *5*, 4357−4366.
(11) Ayton, G. S.; Noid, W. G.; Voth, G. A. *Curr. Opin. Struct. Biol.* **2007**, *17*, 192−198.
(12) Warshel, A. *Annu. Rev. Biophys. Biomol. Struct.* **2003**, *32*, 425−443.
(13) Neri, M.; Anselmi, C.; Cascalla, M.; Maritan, A.; Carloni, P. *Phys. Rev. Lett.* **2005**, *95*, 218102.
(14) Rzepiela, A. J.; Louhivuori, M.; Peter, C.; Marrink, S. J. *Phys. Chem. Chem. Phys.* **2011**, *13*, 10437−10448.
(15) Riniker, S.; Eichenberger, A. P.; van Gunsteren, W. F. *J. Phys. Chem. B* **2012**, *116*, 8873−8879.
(16) Han, W.; Schulten, K. *J. Chem. Theory Comput.* **2012**, *8*, 4413−4424.
(17) Sokkar, P.; Choi, S. M.; Rhee, Y. M. *J. Chem. Theory Comput.* **2013**, *9*, 3728−3739.
(18) Wassenaar, T. A.; Ingólfsson, H. I.; Priess, M.; Marrink, S. J.; Schaefer, L. V. *J. Phys. Chem. B* **2013**, *117*, 3516−3530.
(19) Sokkar, P.; Choi, S. M.; Rhee, Y. M. *J. Chem. Theory Comput.* **2013**, *9*, 3728−3739.
(20) Gonzalez, H. C.; Darré, L.; Pantano, S. *J. Phys. Chem. B* **2013**, *117*, 14438−14448.
(21) Abrams, C. F. *J. Chem. Phys.* **2005**, *123*, 234101.
(22) Nielsen, S. O.; Moore, P. B.; Ensing, B. *Phys. Rev. Lett.* **2010**, *105*, 237802.
(23) Heyden, A.; Truhlar, D. G. *J. Chem. Theory Comput.* **2008**, *4*, 217−221.
(24) Potestio, R.; Fritsch, S.; Español, P.; Delgado-Buscalioni, R.; Kremer, K.; Everaers, R.; Donadio, D. *Phys. Rev. Lett.* **2013**, *110*, 108301.
(25) Potestio, R.; Español, P.; Delgado-Busclioni, R.; Everaers, R.; Kremer, K.; Donadio, D. *Phys. Rev. Lett.* **2013**, *111*, 060601.
(26) Praprotnik, M.; Delle Site, L.; Kremer, K. *J. Chem. Phys.* **2005**, *123*, 224106.

(27) Delgado-Buscalioni, R.; Kremer, K.; Praprotnik, M. *J. Chem. Phys.* **2008**, *128*, 114110.
(28) Poma, A. B.; Delle Site, L. *Phys. Rev. Lett.* **2010**, *104*, 250201.
(29) Praprotnik, M.; Poblete, S.; Kremer, K. *J. Stat. Phys.* **2011**, *145*, 946−966.
(30) Wang, H.; Schuette, C.; Delle Site, L. *J. Chem. Theory Comput.* **2012**, *8*, 2878−2887.
(31) Wang, H.; Hartmann, C.; Schuette, C.; Delle Site, L. *Phys. Rev. X* **2013**, *3*, 011018.
(32) Fuhrmans, M.; Sanders, B. P.; Marrink, S. J.; de Vries, A. H. *Theor. Chem. Acc.* **2010**, *125*, 335−344.
(33) Nagarajan, A.; Junghans, C.; Matysiak, S. *J. Chem. Theory Comput.* **2013**, *9*, 5168−5175.
(34) Oostenbrink, C.; Villa, A.; Mark, A. E.; van Gunsteren, W. F. *J. Comput. Chem.* **2004**, *25*, 1656−76.
(35) Poblete, S.; Praprotnik, M.; Kremer, K.; Delle Site, L. *J. Chem. Phys.* **2010**, *132*, 114101.
(36) Fritsch, S.; Poblete, S.; Junghans, C.; Ciccotti, G.; Delle Site, L.; Kremer, K. *Phys. Rev. Lett.* **2012**, *108*, 170602.
(37) Junghans, C.; Praprotnik, M.; Kremer, K. *Soft Matter* **2008**, *4*, 156−161.
(38) Soddemann, T.; Dunweg, B.; Kremer, K. *Phys. Rev. E* **2003**, *68*, 046702.
(39) Halverson, J. D.; Brandes, T.; Lenz, O.; Arnold, A.; Bevc, S.; Starchenko, V.; Kremer, K.; Stuehn, T.; Reith, D. *Comput. Phys. Commun.* **2013**, *184*, 1129−1149.
(40) Zavadlav, J.; Melo, M. N.; Marrink, S. J.; Praprotnik, M. *J. Chem. Phys.* **2014**, *140*, 054114.
(41) Miyamoto, S.; Kollman, P. A. *J. Comput. Chem.* **1992**, *13*, 952−962.
(42) Neumann, M. *J. Chem. Phys.* **1985**, *82*, 5663−5672.
(43) Neumann, M. *Mol. Phys.* **1983**, *50*, 841−858.
(44) Fritsch, S.; Junghans, C.; Kremer, K. *J. Chem. Theory Comput.* **2012**, *8*, 398−403.
(45) Ruehle, V.; Junghans, C.; Lukyanov, A.; Kremer, K.; Andrienko, D. *J. Chem. Theory Comput.* **2009**, *5*, 3211−3223.
(46) Jedlovszky, P.; Vincze, A.; Horvai, G. *Phys. Chem. Chem. Phys.* **2007**, *6*, 1874−1879.
(47) Praprotnik, M.; Matysiak, S.; Delle Site, L.; Kremer, K.; Clementi, C. *J. Phys.: Condens. Matter* **2007**, *19*, 292201.
(48) Smith, P. E.; van Gunsteren, W. F. *J. Chem. Phys.* **1994**, *100*, 3169−3174.
(49) Dunweg, B.; Kremer, K. *J. Chem. Phys.* **1993**, *99*, 6983−6997.
(50) Yeh, I. C.; Hummer, G. *J. Phys. Chem. B* **2004**, *108*, 15873−15879.
(51) van der Spoel, D.; van Maaren, P. J.; Berendsen, H. J. C. *J. Chem. Phys.* **1998**, *108*, 10220−10230.
(52) Goga, N.; Rzepiela, A. J.; de Vries, A. H.; Marrink, S. J.; Berendsen, H. J. C. *J. Chem. Theory Comput.* **2012**, *8*, 3637−3649.
(53) Dima, R. I.; Thirumalai, D. *J. Phys. Chem. B* **2004**, *108*, 6564−6570.